Articles

Syntheses, Structural Characterization, and Luminescence Behavior of Face-to-Face Diplatinum(II) Alkynyl Complexes

Vivian Wing-Wah Yam,* Chi-Kuen Hui, Keith Man-Chung Wong, Nianyong Zhu, and Kung-Kai Cheung

Centre for Carbon-Rich Molecular and Nano-scale Metal-Based Materials Research and Department of Chemistry, The University of Hong Kong, Pokfulam Road, Hong Kong, People's Republic of China

Received February 7, 2002

A series of luminescent face-to-face dinuclear platinum(II) alkynyl complexes, $[Pt_2(\mu\text{-dppm})_2(C{\equiv}CR)_4]$ (R = C_6H_4-Cl-*p*, C_6H_4-NO_2-*p*, $SiMe_3$), and a mixed-metal platinum(II)−silver(I) complex, $[Pt_2(\mu\text{-dppm})_2(C{\equiv}CPh)_4{\cdot}\{Ag(MeCN)\}_2](BF_4)_2$, were synthesized and characterized by both spectroscopy and X-ray crystallography. Their luminescence behavior were studied and the nature of the emission origin was elucidated by comparison studies involving the perturbation of Pt···Pt distances as well as the π-accepting ability of the alkynyl group through a systematic variation of the nature of the alkynyl moieties and metal ion encapsulation.

Introduction

The study of the spectroscopic and luminescence behavior of discrete dinuclear d^8-d^8 complexes has attracted growing attention since the last few decades, which is in part due to the interesting observation of weak metal−metal interactions. A number of dinuclear d^8-d^8 metal complexes with well-defined metal−metal distances have been reported, and their unique spectroscopic features in the absorption and emission spectra have been extensively studied.[1] Earlier works include those of $[Pt_2(pop)_4]^{4-}$,[1a] $[Rh_2(\mu\text{-dppm})_2(RNC)_4]^{2+}$,[1b] $[Rh_2(\mu\text{-dppm})_2(CO)_2Cl_2]$,[1c] $[Pt_2(\mu\text{-dppm})_2(CN)_4]$,[1d] and a number of square planar rhodium(I) and platinum(II) complexes[2] such as $[Rh(CNR)_4]^+$,[2c] $[Pt(bpy)X_2]$ (X = Cl, CN),[2d−f] and $[Pt(4,7\text{-}Ph_2phen)(CN)_2]$.[2g] The unique spectroscopic properties in these complexes have been suggested to be associated with the presence of weak metal−metal interactions.[1,2] As an extension of our previous work on A-frame diplatinum(II) alkynyl complexes,[3] a program was launched to investigate the luminescence properties of the face-to-face diplatinum(II) alkynyl complex $[Pt_2(\mu\text{-dppm})_2(C{\equiv}CPh)_4]$, which was first synthesized by Pringle and Shaw.[4] It is hoped that through a systematic variation of the alkynyl ligands with different π-accepting abilities, a series of structurally related analogues could be synthesized, which would provide insights into the role played by the

* Corresponding author. Fax: (852) 2857-1586. E-mail: wwyam@hku.hk.

(1) (a) Roundhill, D. M.; Gray, H. B.; Che, C. M. *Acc. Chem. Res.* **1989**, *22*, 55. (b) Balch, A. L. *J. Am. Chem. Soc.* **1976**, *98*, 8049. (c) Inga M.; Kenney, S.; Kenney, J. W.; Crosby, G. A. *Organometallics* **1986**, *5*, 230. (d) Che, C. M.; Yam, V. W. W.; Wong, W. T.; Lai, T. F. *Inorg. Chem.* **1989**, *28*, 2908. (e) Smith, D. C.; Gray, H. B. *Coord. Chem. Rev.* **1990**, *100*, 169. (f) Yip, H. K.; Che, C. M.; Zhou, Z. Y.; Mak, T. C. W. *J. Chem. Soc., Chem. Commun.* **1992**, 1369. (g) Striplin, D. R.; Crosby, G. A. *J. Phys. Chem.* **1995**, *99*, 7977. (h) Lewis, N. S.; Mann, K. R.; Gordon, J. G., II; Gray, H. B. *J. Am. Chem. Soc.* **1976**, *98*, 7461.

(2) (a) Vogler, A.; Kunkely, H. *J. Am. Chem. Soc.* **1981**, *103*, 1559. (b) Lechner, A.; Gliemann, G. *J. Am. Chem. Soc.* **1989**, *111*, 7469. (c) Mann, K. R.; Lewis N. S.; Williams R. M.; Gray, H. B.; Gordon, J. G., II. *Inorg. Chem.* **1978**, *17*, 828. (d) Che, C. M.; He, L. Y.; Poon, C. K.; Mak, T. C. W. *Inorg. Chem.* **1989**, *28*, 3081. (e) Mann, K. R.; Gordon, J. G., II; Gray, H. B. *J. Am. Chem. Soc.* **1975**, *97*, 3553. (f) Miskowski, V. M.; Houlding, V. H. *Inorg. Chem.* **1989**, *28*, 1529. (g) Kunkely, H.; Vogler, A. *J. Am. Chem. Soc.* **1990**, *112*, 5625. (h) Yersin, H.; Humbs, W.; Strasser, J. *Coord. Chem. Rev.* **1997**, *159*, 325.

(3) (a) Yam, V. W. W. *J. Photochem. Photobiol. A* **1997**, *106*, 75. (b) Yam, V. W. W.; Lo, K. K. W.; Fung, W. K. M.; Wang, C. R. *Coord. Chem. Rev.* **1998**, *171*, 17. (c) Yam, V. W. W.; Lo, K. K. W. *Chem. Soc. Rev.* **1999**, *28*, 323. (d) Yam, V. W. W.; Lo, K. K. W.; Wong, K. M. C. *J. Organomet. Chem.* **1999**, *578*, 3. (e) Yam, V. W. W.; Chan, L. P.; Lai, T. F. *Organometallics* **1993**, *12*, 2197. (f) Yam, V. W. W.; Yeung, P. K. Y.; Chan, L. P.; Kwok, W. M.; Phillips, D. L.; Yu, K. L.; Wong, R. W. K.; Yan, H.; Meng, Q. J. *Organometallics* **1998**, *17*, 2590.

(4) (a) Pringle, P. G.; Shaw, B. L. *J. Chem. Soc., Chem. Commun.* **1982**, 581. (b) Langrich, C. R.; McEwan, D. M.; Pringle, P. G.; Shaw, B. L. *J. Chem. Soc., Dalton Trans.* **1983**, 2487.

(5) Yam, V. W. W.; Yu, K. L.; Wong, K. M. C.; Cheung, K. K. *Organometallics* **2001**, *20*, 721.

(6) Ames, D. E.; Bull, D.; Takundwa, C. *Synthesis* **1981**, 364.

(7) Brown, M. P.; Puddephatt, R. J.; Rashidi, M.; Seddon, K. R. *J. Chem. Soc., Dalton Trans.* **1977**, 951.

(8) (a) *DENZO*: In *The HKL Manual-A description of programs DENZO, XDISPLAYF, and SCALEPACK*; written by Gewirth, D. with the coorperation of the program authors Z. Otwinowski and W. Minor, Yale University, New Haven, CT, 1995. (b) *PATTY*: Beurskens, P. T.; Admiraal, G.; Beurskens, G.; Bosman, W. P.; Garcia-Granda, S.; Gould, R. O.; Smits J. M. M.; Smykalla, C. *The DIRDIF program system*; Technical Report of the Crystallography Laboratory; University of Nijmegen: The Netherlands, 1992. (c) *TeXsan*: *Crystal Structure Analysis Package*; Molecular Structure Corporation: The Woodlands, TX, 1985 &, 1992. (d) *SHELXS97*: Shekdrick, G. M. *SHELX97*: Programs for Crystal Structure Analysis (Release 97-2); University of Goetingen: Germany, 1997. (e) *SHELXL97*: Shekdrick, G. M. *SHELX97*: Programs for Crystal Structure Analysis (Release 97-2); University of Goetingen: Germany, 1997.

10.1021/om020093o CCC: $22.00
Publication on Web 09/14/2002

alkynyl ligands as well as their relation to the extent of metal−metal interactions in the spectroscopic and excited-state properties of this class of complexes. Herein we report the synthesis, luminescence behavior, and structural characterization of a series of face-to-face dinuclear platinum(II) alkynyl complexes, $[Pt_2(\mu\text{-dppm})_2(C{\equiv}CR)_4]$ (R = C_6H_4-Cl-*p* **1**, C_6H_4-NO_2-*p* **2**, $SiMe_3$ **3**). Attempts to correlate the effect of the Pt···Pt distance with the nature of the alkynyl moieties and the luminescence behavior have been made. A related mixed-metal tetranuclear complex, $[Pt_2(\mu\text{-dppm})_2(C{\equiv}CPh)_4{\cdot}\{Ag(MeCN)\}_2](BF_4)_2$ (**4**), which is an analogue of $[Pt_2(\mu\text{-dppm})_2(C{\equiv}CPh)_4{\cdot}\{Cu(MeCN)\}_2](PF_6)_2$ that was previously reported by us,[5] has also been synthesized and structurally characterized. This should provide further insights into the nature of the excited-state origin by the perturbation of the metal−metal distance as well as the π-accepting ability of the alkynyl group via Ag(I) encapsulation.

Experimental Section

Materials. The ligand bis(diphenylphosphino)methane (dppm) and $[Pt(cod)Cl_2]$ were purchased from Strem Chemicals Inc. ^{n}BuLi in *n*-hexane (2.5 M), 4-chlorophenylacetylene, and $[Ag(MeCN)_4]BF_4$ were purchased from Aldrich Chemical Co. Inc. Trimethylsilylacetylene was purchased from GFS Chemical Co. Ltd. 4-Nitrophenylacetylene,[6] [Pt(dppm-*P*,*P*′)Cl_2],[7] and $[Pt_2(\mu\text{-dppm})_2(C{\equiv}CPh)_4]$[4] were prepared according to literature procedures. All solvents were purified and distilled under N_2 using previously used standard procedures.

Syntheses of Dinuclear Platinum(II) Alkynyl Complexes and Related Mixed-Metal Complexes. $[Pt_2(\mu\text{-dppm})_2(C{\equiv}CC_6H_4Cl\text{-}p)_4]$, 1. This was prepared by modifications of a method for $[Pt_2(\mu\text{-dppm})_2(C{\equiv}CPh)_4]$ described in the literature.[4] To a solution of lithium 4-chlorophenylacetylide, prepared in situ by treating $HC{\equiv}CC_6H_4Cl$-*p* (0.066 g, 0.48 mmol) in THF (10 mL) with ^{n}BuLi (0.19 mL, 0.48 mmol) at 0 °C, was added [Pt(dppm-*P*,*P*′)Cl_2] (0.15 g, 0.23 mmol) in benzene (10 mL). The mixture was stirred at −78 °C for half an hour and then heated to reflux for 24 h. The resulting mixture was evaporated to dryness and triturated with methanol to give a yellow solid residue. Recrystallization from dichloromethane−acetone afforded **1** as air-stable greenish-yellow crystals. Yield: 0.16 g (80%). ^{1}H NMR (400 MHz, CD_2Cl_2, 298 K, relative to $SiMe_4$): δ 4.65 (m, 4H, PCH_2P), 6.36 (d, 8H, phenyl protons *ortho* to C≡C, J = 8.4 Hz), 6.78 (d, 8H, phenyl protons *meta* to C≡C, J = 8.4 Hz), 7.09 (t, 16H, phenyl protons *meta* to P, J = 7.2 Hz), 7.23 (t, 8 H, phenyl protons *para* to P, J = 7.2 Hz), 7.78 (d, 16H, phenyl protons *ortho* to P, J = 7.2 Hz). ^{31}P{^{1}H} NMR (161 MHz, CD_2Cl_2, 298 K, relative to 85% H_3PO_4): δ 1.99 (s, J(Pt−P) = 2738 Hz). IR (Nujol mull), ν(C≡C): 2106 cm^{-1} (s). Positive FAB-MS at *m*/*z*: 1701 {M}$^+$. Anal. Calcd for $C_{82}H_{60}P_4Cl_4Pt_2$: C, 57.89; H, 3.55. Found: C, 57.58; H, 3.48.

$[Pt_2(\mu\text{-dppm})_2(C{\equiv}CC_6H_4NO_2\text{-}p)_4]$, 2. This was similarly prepared but with slight modifications. To a solution of lithium 4-nitrophenylacetylide, prepared in situ by treating $HC{\equiv}CC_6H_4NO_2$-*p* (0.21 g, 1.44 mmol) in THF (50 mL) with ^{n}BuLi (0.57 mL, 1.44 mmol) at −78 °C, was added [Pt(dppm-*P*,*P*′)Cl_2] (0.37 g, 0.569 mmol) in benzene (50 mL). The mixture was stirred at −78 °C for half an hour and then heated under reflux for 24 h. The resulting mixture was evaporated to dryness and purified by column chromatography on silica gel using acetone as eluent to remove a dark red impurity, followed by elution with dichloromethane to obtain the orange-yellow fraction. Removal of solvent gave **2** as an orange-yellow solid. Recrystallization by vapor diffusion of diethyl ether to the concentrated dichloromethane solution of the product afforded **2** as air-stable orange-yellow crystals. Yield: 0.10 g (21%). ^{1}H NMR (400 MHz, CD_2Cl_2, 298 K, relative to $SiMe_4$): δ 4.59 (m, 4H, PCH_2P), 6.41 (d, 8H, phenyl protons *ortho* to the C≡C, J = 8.9 Hz), 7.12 (t, 16H, phenyl protons *meta* to P, J = 7.4 Hz), 7.29 (t, 16H, phenyl protons *para* to P, J = 7.4 Hz), 7.65 (d, 8H, phenyl protons *meta* to the C≡C, J = 8.9 Hz), 7.76 (d, 16H, phenyl protons *ortho* to P, J = 7.4 Hz). ^{31}P{^{1}H} NMR (161 MHz, CD_2Cl_2, 298 K, relative to 85% H_3PO_4): δ 2.51 (s, J(Pt−P) = 2746 Hz). IR (Nujol mull), ν(C≡C): 2104 cm^{-1} (s). Positive FAB-MS at *m*/*z*: 1743 {M}$^+$. Anal. Calcd for $C_{82}H_{60}N_4O_8P_4Pt_2{\cdot}0.5CH_2Cl_2$: C, 55.48; H, 3.44; N, 3.13. Found: C, 55.57; H, 3.53; N, 2.91.

Synthesis of $[Pt_2(\mu\text{-dppm})_2(C{\equiv}CSiMe_3)_4]$, 3. This was similarly prepared but with slight modifications. To a solution of lithium trimethylsilylacetylide, prepared in situ by treating $Me_3SiC{\equiv}CH$ (0.061 g, 0.61 mmol) in THF (10 mL) with ^{n}BuLi (0.25 mL, 0.61 mmol) at −78 °C, was added [Pt(dppm-*P*,*P*′)Cl_2] (0.20 g, 0.30 mmol) in benzene (10 mL). The mixture was stirred at −78 °C for half an hour and then heated under reflux for 24 h. The resulting mixture was evaporated to dryness and triturated with methanol to give a solid residue. Recrystallization by addition of acetone to the concentrated dichloromethane solution afforded **3** as air-stable pale yellow crystals. Yield: 0.12 g (58%). ^{1}H NMR (400 MHz, CD_2Cl_2, 298 K, relative to $SiMe_4$): δ 0.26 (s, 36H, −$SiMe_3$), 4.89 (m, 4H, PCH_2P), 7.36 (t, 16H, phenyl protons *meta* to P, J = 7.6 Hz), 7.47 (t, 16H, phenyl protons *para* to P, J = 7.6 Hz), 7.96 (d, 16H, phenyl protons *ortho* to P, J = 7.6 Hz). ^{31}P{^{1}H} NMR (161 MHz, CD_2Cl_2, 298 K, relative to 85% H_3PO_4): δ 0.96 (s, J(Pt−P) = 2819 Hz). IR (Nujol mull), ν(C≡C): 2034 cm^{-1} (s). Positive FAB-MS at *m*/*z*: 1547 {M}$^+$. Anal. Calcd for $C_{70}H_{80}P_4Pt_2Si_4$: C, 54.32; H, 5.21. Found: C, 54.38; H, 5.24.

$[Pt_2(\mu\text{-dppm})_2(C{\equiv}CPh)_4{\cdot}\{Ag(MeCN)\}_2](BF_4)_2$, 4. To a yellow suspension of $[Pt_2(\mu\text{-dppm})_2(C{\equiv}CPh)_4]$ (0.080 g, 0.05 mmol) in dichloromethane (10 mL) was added dropwise $[Ag(MeCN)_4]BF_4$ (0.036 g, 0.10 mmol) in acetone solution (10 mL). The reaction mixture immediately turned to clear greenish-yellow solution and was allowed to stir for 30 min. After removal of solvent under vacuum, a greenish-yellow solid was obtained. Subsequent recrystallization from acetone−*n*-hexane afforded **4** as air-stable greenish-yellow rod-shaped crystals. Yield: 0.08 g (82%). ^{1}H NMR (400 MHz, CD_2Cl_2, 298 K, relative to $SiMe_4$): δ 1.35 (s, 6H, MeCN), 4.65 (m, 4H, PCH_2P), 6.20 (d, 8H, phenyl protons *ortho* to C≡C, J = 7.2 Hz), 7.05 (t, 8H, phenyl protons *meta* to C≡C, J = 7.2 Hz), 7.25 (t, 4H, phenyl protons *para* to C≡C, J = 7.2 Hz), 7.34 (t, 16H, phenyl protons *meta* to P, J = 6.9 Hz), 7.43 (t, 8H, phenyl protons *para* to P, J = 6.9 Hz), 7.94 (d, 16H, phenyl protons *ortho* to P, J = 6.9 Hz). ^{31}P{^{1}H} NMR (202 MHz, CD_2Cl_2, 298 K, relative to 85% H_3PO_4): δ 4.97 (s, J(Pt−P) = 2588 Hz). IR (Nujol mull), ν(C≡C): 2036 cm^{-1} (w). Positive ESI-MS: ion clusters at *m*/*z* 1845 {M − Ag − 2MeCN}$^+$. Anal. Calcd for **4** $C_{86}H_{70}Ag_2B_2F_8N_2P_4Pt_2$: C, 50.76; H, 3.46; N 1.38. Found: C, 51.04; H, 3.28; N 1.53.

Physical Measurements and Instrumentation. UV−visible spectra were obtained on a Hewlett-Packard 8452A diode array spectrophotometer, IR spectra as Nujol mulls on a Bio-Rad FTS-7 Fourier transform infrared spectrophotometer (4000−400 cm^{-1}), positive ion FAB mass spectra on a Finnigan MAT95 mass spectrometer, and positive ESI mass spectra on a Finnigan LCQ mass spectrometer. ^{1}H NMR spectra, with chemical shifts reported relative to tetramethylsilane, and ^{31}P{^{1}H} NMR spectra with chemical shifts relative to 85% H_3PO_4 external reference were recorded on Bruker DPX-300, Bruker Avance 400, and Bruker DRX-500 NMR spectrometers. Elemental analyses were performed on a Carlo Erba 1106 elemental analyzer at the Institute of Chemistry in Beijing, Chinese Academy of Sciences. Steady-state emission and excitation spectra at room temperature and at 77 K were obtained on a Spex Fluorolog-2 model F111 fluorescence spectrophotometer with or without Corning filters. The 77 K

solid-state emission and excitation spectra were recorded with solid samples loaded in a quartz tube inside a quartz-walled optical Dewar flask filled with liquid nitrogen. For solution emission and excitation spectral studies, the solutions were prepared in a 10 mL Pyrex bulb connected to a sidearm 1 cm quartz cuvette and sealed from the atmosphere by a Rotaflo HP6/6 quick-release Teflon stopper. The solutions were rigorously degassed with no fewer than four freeze−pump−thaw cycles. Emission lifetime measurements were performed using a conventional laser system. The excitation source was the 355 nm output (third harmonic) of a Spectra-Physics Quanta-Ray Q-switched GCR-150-10 pulsed Nd:YAG laser. Luminescence decay signals were recorded on a Tektronix model TDS620A digital oscilloscope and analyzed using a program for exponential fits. Time-resolved emission spectra were recorded on an Oriel Instruments intensified charge-coupled device (ICCD) detector (Model DH520) and were analyzed using the InstaSpec V software. The excitation source is the same laser system as that used for lifetime measurement. The emission signal was collected by an optical fiber and dispersed onto the CCD detector with an Oriel MultiSpec 115 imaging spectrograph (Model 77480). A Stanford Research Systems (SRS) delay generator (Model DG 535) was used to produce the transistor-transistor logic (TTL) pulse needed to operate the intensifier gating electronics in the detector head. The external trigger input of the delay generator was connected to the laser's prepulse trigger output. The delay generator was controlled via an IBM AT APIB (IEEE 488) card interfaced with an IBM-compatible Pentium personal computer to allow the InstaSpec V software to send commands to control the width and delay of the TTL pulse. The system was operated at −15 °C by the single stage system in order to reduce the dark current signal.

Crystal Structure Determination. All crystal structures were determined on a MAR diffractometer at 28 °C with a 300 mm image plate detector using graphite-monochromatized Mo Kα radiation ($\lambda = 0.71073$ Å). The images were interpreted and intensities integrated using the program DENZO.[8a] Crystal structure of **1** was solved on the basis of systematic absences and a statistical analysis of intensity distribution, and the successful refinement of the structure was solved by Patterson methods and expanded by the Fourier method (PATTY[8b]) and refinement by full-matrix least-squares using the software package TeXsan[8c] on a Silicon Graphics Indy computer. Crystal structures of **2**−**4** were solved by direct methods employing the SHELXS-97 program[8d] on a PC. Pt atoms were located according to the direct methods. The positions of the other non-hydrogen atoms were found after successful refinement by full-matrix least-squares using the program SHELXL-97[8e] on a PC.

Crystal data for $[C_{82}H_{64}P_4Pt_2\cdot 2CH_2Cl_2]$, $1\cdot 2CH_2Cl_2$: fw = 1871.13, monoclinic, space group $P2_1/n$ (No. 14), a = 12.406(2) Å, b = 22.845(3) Å, c = 13.911(2) Å, β = 105.99(2)°, V = 3790(1) Å^3, $Z = 2$, $D_c = 1.639$ g cm^{-3}, μ(Mo Kα) = 40.83 cm^{-1}, $F(000) = 1840$, $T = 301$ K. A yellow crystal of dimensions 0.20 × 0.10 × 0.10 mm inside a glass capillary was used for data collection. A total of 7328 unique reflections were obtained from a total of 6996 measured reflections ($R_{int} = 0.050$). A total of 5755 reflections with $I > 3\sigma(I)$ were observed and used in the structural analysis. Convergence for 442 variable parameters by least-squares refinement on F with $w = 4F_o^2/\sigma^2(F_o^2)$, where $\sigma^2(F_o^2) = [\sigma^2(I) + (0.040F_o^2)^2]$ for 5755 reflections with $I > 3\sigma(I)$, was reached at $R = 0.035$ and $R_w = 0.053$ with a goodness-of-fit of 1.46. $(\Delta/\sigma)_{max} = 0.04$ except for the C atoms of the solvent molecules. The final difference Fourier map was featureless, with maximum positive and negative peaks of 1.29 and 1.16 e Å^{-3} respectively.

Crystal data for $[C_{82}H_{60}N_4O_8P_4Pt_2\cdot 4CH_2Cl_2]$, $2\cdot 4CH_2Cl_2$: fw = 2083.10, monoclinic, space group $P2_1/n$ (No. 14), a = 14.390(2) Å, b = 15.992(2) Å, c = 18.842(2) Å, β = 104.09(2)°, V = 4205.6(9) Å^3, $Z = 2$, $D_c = 1.645$ g cm^{-3}, μ(Mo Kα) = 37.11 cm^{-1}, $F(000) = 2056$, $T = 301$ K. A reddish yellow crystal of dimensions 0.40 × 0.40 × 0.15 mm inside a glass capillary was used for data collection. A total of 7752 unique reflections were obtained from a total of 24 875 measured reflections ($R_{int} = 0.058$). A total of 6624 reflections with $I > 4\sigma(F_o)$ were observed and used in the structural analysis. Convergence for 505 variable parameters by full-matrix least-squares refinement on F with $w = 4F_o^2/\sigma^2(F_o^2)$, where $\sigma^2(F_o^2) = [\sigma^2(I) + (0.029F_o^2)^2]$ for 6624 reflections with $I > 4\sigma(I)$, was reached at $R = 0.034$ and $R_w = 0.096$ with a goodness-of-fit of 1.095. $(\Delta/\sigma)_{max} = -0.01$, av 0.001. The final difference Fourier map shows maximum peaks and holes of 0.692 and −1.94 e Å^{-3} respectively.

Crystal data for $[C_{70}H_{80}P_4Pt_2Si_4]$, 3: fw = 1547.76, triclinic, space group $P\bar{1}$, a = 11.664(2) Å, b = 11.845(2) Å, c = 14.093(3) Å, α = 108.47(3)°, β = 100.62(3)°, γ = 103.75(3)°, V = 1721.3(6) Å^3, $Z = 1$, $D_c = 1.493$ g cm^{-3}, μ(Mo Kα) = 42.60 cm^{-1}, $F(000) = 772$, $T = 301$ K. A pale yellow crystal of dimensions 0.40 × 0.30 × 0.25 mm inside a glass capillary was used for data collection. A total of 5714 unique reflections were obtained from a total of 10 306 measured reflections ($R_{int} = 0.072$). A total of 5181 reflections with $I > 4\sigma(F_o)$ were observed and used in the structural analysis. Convergence for 361 variable parameters by full-matrix least-squares refinement on F with $w = 4F_o^2/\sigma^2(F_o^2)$, where $\sigma^2(F_o^2) = [\sigma^2(I) + (0.029F_o^2)^2]$ for 5181 reflections with $I > 4\sigma(I)$, was reached at $R = 0.049$ and $R_w = 0.121$ with a goodness-of-fit of 1.053. $(\Delta/\sigma)_{max} = -0.01$, av 0.001. The final difference Fourier map shows maximum peaks and holes of 1.248 and −1.705 e Å^{-3}, respectively.

Crystal data for $[C_{86}H_{70}Ag_2B_2F_8N_2P_4Pt_2]$, 4: fw = 2034.86, orthorhombic, space group $Pnn2$, a = 20.211(2) Å, b = 20.214(2) Å, c = 19.308(2) Å, V = 7888.2(14) Å^3, $Z = 4$, $D_c = 1.713$ g cm^{-3}, μ(Mo Kα) = 41.71 cm^{-1}, $F(000) = 3968$, $T = 301$ K. A yellow crystal of dimensions 0.40 × 0.30 × 0.15 mm inside a glass capillary was used for data collection. A total of 9713 unique reflections were obtained from a total of 15 209 measured reflections ($R_{int} = 0.072$). A total of 7408 reflections with $I > 4\sigma(F_o)$ were observed and used in the structural analysis. Convergence for 889 variable parameters by full-matrix least-squares refinement on F with $w = 4F_o^2/\sigma^2(F_o^2)$, where $\sigma^2(F_o^2) = [\sigma^2(I) + (0.029F_o^2)^2]$ for 7408 reflections with $I > 4\sigma(I)$, was reached at $R = 0.040$ and $R_w = 0.099$ with a goodness-of-fit of 1.023. $(\Delta/\sigma)_{max} = 3$ for BF_4^- anions, 0.5 for some C atoms, and most are lower than 0.01, av 0.039. The final difference Fourier map shows maximum peaks and holes of 0.939 and −0.881 e Å^{-3}, respectively.

Crystal and structure determination data as well as the selected bond distances and bond angles of **1**−**4** are collected in Tables 1 and 2, respectively.

Results and Discussion

In the synthesis of the face-to-face dinuclear platinum(II) alkynyl complexes, LiC≡CR, generated in situ from the corresponding RC≡CH and ^{n}BuLi, was used to react with [Pt(dppm-*P*,*P*′)Cl$_2$] at −78 °C. Unlike in the preparation of [Pt$_2$(μ-dppm)$_2$(C≡CPh)$_4$], where the LiC≡CPh generated is relatively stable, the LiC≡CR formed in the present work were comparatively less stable at room temperature, especially for the more electron-deficient RC≡CH. Thus the preparations of the related complexes were performed at −78 °C instead of at room temperature to produce a higher yield.

Similar to the analogue complex, [Pt$_2$(μ-dppm)$_2$(C≡CPh)$_4$], **1** and **3** are not very soluble in common organic solvents but only dissolve slowly in dichloromethane, while **2** is soluble in both acetone and dichloromethane. For the purification of **1** and **3**, the

Table 1. Crystal and Structure Determination Data

	1	**2**	**3**	**4**
formula	$C_{82}H_{60}P_4Cl_4Pt_2 \cdot 2CH_2Cl_2$	$C_{82}H_{68}N_4O_8P_4Pt_2 \cdot 4CH_2Cl_2$	$C_{70}H_{80}P_4Pt_2Si_4$	$C_{86}H_{70}Ag_2B_2F_{12}N_2P_4Pt_2$
fw	1871.13	2083.10	1547.76	2034.86
T, °C	28	28	28	28
a, Å	12.406(2)	14.390(2)	11.664(2)	20.211(2)
b, Å	22.845(3)	15.992(2)	11.846(2)	20.214(2)
c, Å	13.911(2)	18.842(2)	14.093(3)	19.308(2)
α, deg			108.47(3)	
β, deg	105.99(2)	104.09(2)	100.62(3)	
γ, deg			103.75(3)	
V, Å^3	3790(1)	4205.6(9)	1721.3(6)	7888.2(14)
cryst syst	monoclinic	monoclinic	triclinic	orthorhombic
space group	$P2_1/n$	$P2_1/n$	$P\bar{1}$	$Pnn2$
Z	2	2	1	4
F(000)	1840	2056	772	3968
D_c, g cm^{-3}	1.639	1.645	1.493	1.713
cryst color/shape	yellow crystal	reddish yellow crystal	yellow crystal	yellow crystal
cryst dimens, mm	0.20 × 0.10 × 0.10	0.40 × 0.4 × 0.15	0.40 × 0.30 × 0.25	0.40 × 0.30 × 0.15
λ, Å (graphite monochromated, Mo Kα)	0.71073	0.71073	0.71073	0.71073
μ, cm^{-1}	40.83	40.01	38.45	40.01
collection range	$2\theta_{max} = 51.1°$; h: 0 to 12, k: 0 to 42, l: −25 to 25	$2\theta_{max} = 51.1°$; h: −16 to 17, k: −19 to 19, l: −22 to 22	$2\theta_{max} = 51.1°$; h: −13 to 12, k: −14 to 14, l: −16 to 17	$2\theta_{max} = 51.1°$; h: −24 to 20, k: −9 to 23, l: −23 to 22
data collection mode	2.8° oscillation (60 images) × 120 mm distance × 540 s exposure	2.0° oscillation (82 images) × 120 mm distance × 300 s exposure	2.5° oscillation (100 images) × 120 mm distance × 300 s exposure	2.0° oscillation (33 images) × 120 mm distance × 300 s exposure
no. of data collected	6996	24 875	10 306	15 209
no. of unique data	5755	7752	5714	9713
R_{int}	0.045	0.058	0.072	0.0328
no. of data used in refinement, m	5755 ($I > 3\sigma(I)$)	6624 ($I > 4\sigma(I)$)	5181 ($I > 4\sigma(I)$)	7408 ($I > 4\sigma(I)$)
no. of params refined, p	442	505	361	889
R	0.035	0.034	0.049	0.040
R_w	0.053	0.096	0.121	0.099
S	1.46	1.10	1.053	1.023
max. shift (shift/error)$_{max}$	0.01	0.001	0.001	0.01 except for the some C atoms and BF_4^- anions
residual extrema in final diff map, e Å^{-3}	+1.29, −1.16	+0.692, −1.938	+1.25, −1.71	+0.939, −0.881

reaction mixtures were triturated with methanol, followed by recrystallization from dichloromethane−acetone to afford the product as pure air-stable greenish-yellow crystals. For **2**, the product was purified by column chromatography on silica gel using acetone as eluent to remove a dark red impurity band. A second yellowish orange band containing the desired product was collected by using dichloromethane as eluent.

The structures of **1**−**4** have been determined by X-ray crystallography. Figures 1−4 show the perspective drawings of **1**−**3** and the complex cation of **4**, respectively. All of them show a face-to-face arrangement with two mutually eclipsed platinum atoms bridged by two dppm ligands to form an eight-membered ring (Pt−P−C−P−Pt−P−C−P). Each platinum atom exhibits a distorted square planar geometry with the two alkynyl groups [C−Pt−C, 163.2(3)−172.14(17)°] and the two bridging dppm phosphorus atoms [P−Pt−P, 174.9(4)−177.89(9)°] arranged in a *trans* disposition. Similar face-to-face arrangement has also been observed in a related complex, $[Pt_2(\mu\text{-dppm})_2(CN)_4]$,[1d] in which the four alkynyl groups were replaced by four cyanide ligands. It is noteworthy that the greatest deviation from the idealized square planar geometry for the two alkynyl groups with the platinum atom [C−Pt−C 163.2(3)°] was observed in **3**. Such a phenomenon, together with the observed C≡CSi bond angles of 171.4(7)° and 176.3(7)° that are deviated from the idealized 180°, are believed to be due to the steric bulkiness of the trimethylsilyl groups on the two eclipsed platinum moieties, since the corresponding C≡C−C angles in **1** and **2** are less deviated from the linear arrangement [174.7(5)−178.2(5)°]. In the mixed-metal complex **4**, each of the silver(I) centers is π-bonded to one pair of the preorganized alkynyl groups, which serve as η^2-ligands, and is coordinated to one acetonitrile molecule in a trigonal planar geometry [N(1)−Ag(1)−C(51) 125.2(8)°, N(2)−Ag(2)−C(67) 126.3(8)°]. The C≡C bond distances are in the range 1.186(15)−1.204(12) Å, slightly longer than the C≡C bond distances in the related $[Pt_2(\mu\text{-dppm})_2(C{\equiv}CPh)_4]$ precursor.[4] The weakening of the C≡C bond upon silver(I) coordination is in accord with the π-coordination mode of the alkynyl group and is in agreement with the observation of a lower C≡C stretching frequency {2036(w) cm^{-1} **4**; 2106(s) cm^{-1} $[Pt_2(\mu\text{-dppm})_2(C{\equiv}CPh)_4]$} in the IR spectroscopy. The Pt···Pt distances of **1**−**4** together with the analogue complexes $[Pt_2(\mu\text{-dppm})_2(C{\equiv}CPh)_4]$ and $[Pt_2(\mu\text{-dppm})_2(C{\equiv}CPh)_4\{Cu(MeCN)\}_2](PF_6)_2$ are summarized in Table 3. The short Pt···Pt distances of **1**−**3** in the range 3.25−3.34 Å, which are comparable to that of the related

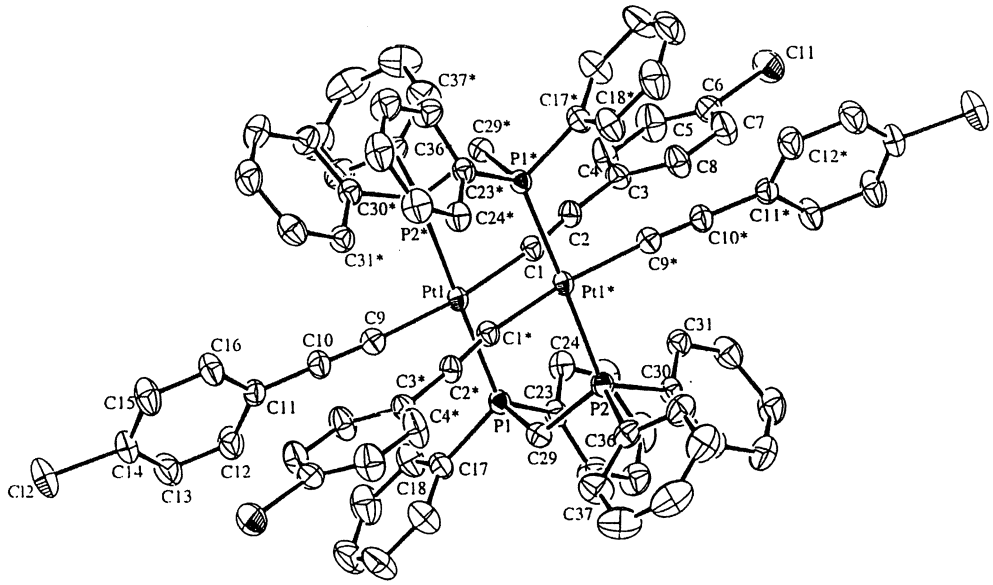

Figure 1. Perspective drawing of **1** with atomic numbering scheme. The H atoms have been omitted for clarity. Thermal ellipsoids are shown at the 30% probability level.

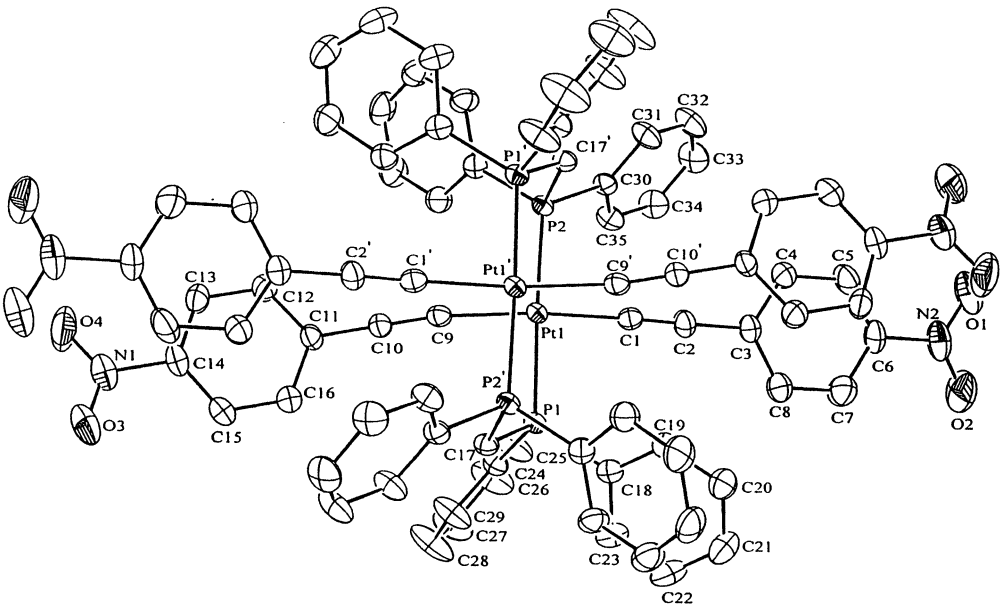

Figure 2. Perspective drawing of **2** with atomic numbering scheme. The H atoms have been omitted for clarity. Thermal ellipsoids are shown at the 30% probability level.

$[Pt_2(\mu\text{-dppm})_2(CN)_4]$ [Pt···Pt 3.301(1) Å],[1d] suggest the presence of a weak Pt···Pt interaction. It is interesting to note that the Pt···Pt distances in $[Pt_2(\mu\text{-dppm})_2(C{\equiv}CR)_4]$ vary with the nature of the alkynyl ligands. In general, shorter Pt···Pt distances were found for complexes with less electron-rich or the more bulky alkynyl groups (R = Ph, 3.437 Å; C_6H_4-Cl-*p*, 3.340 Å; C_6H_4-NO_2-*p*, 3.250 Å; $SiMe_3$, 3.349 Å). The platinum centers, coordinated to the less electron-rich alkynyl ligands with weaker donor strength, would probably favor the occurrence of metal−metal interactions in order to compensate for the reduced electron density, and therefore the Pt···Pt distances decrease. On the other hand, the bulky alkynyl groups such as $Me_3SiC{\equiv}C$ cause the bending of the C−Pt−C bond, forcing the two Pt centers to approach each other more closely due to the steric crowdedness of the two adjacent alkynyl groups. This has been supported by the large deviation observed of the C−Pt−C angle [163.2(3)°] from 180° and the shortening of the Pt···Pt distance (3.349 Å) in **3** relative to $[Pt_2(dppm)_2(C{\equiv}CPh)_4]$ [C−Pt−C 174.4(4)°; Pt···Pt 3.437 Å].[5] Comparatively stronger Pt···Pt interactions were observed in the mixed-metal complexes, **4** [3.0637(9) Å] and $[Pt_2(dppm)_2(C{\equiv}CPh)_4{\cdot}\{Cu(MeCN)\}_2](PF_6)_2$ [3.0124(1) Å],[5] in which the Pt···Pt distances are found to be significantly shorter than that of the precursor complex $[Pt_2(dppm)_2(C{\equiv}CPh)_4]$ [3.437(1) Å].[5] The substantial decrease in the Pt···Pt distances upon metal ion encapsulation is ascribed to the encapsulation of copper(I) or silver(I) metal ions into the cleft between the two alkynyl groups, which pulls the platinum atoms into close proximity as a result of the reduced donor strength of the alkynyl ligands as well as the steric demands required upon copper(I) or silver(I) coordination. The larger ionic radius of the silver(I) ion compared to that of the copper(I) ion as well as the weaker Lewis acid-

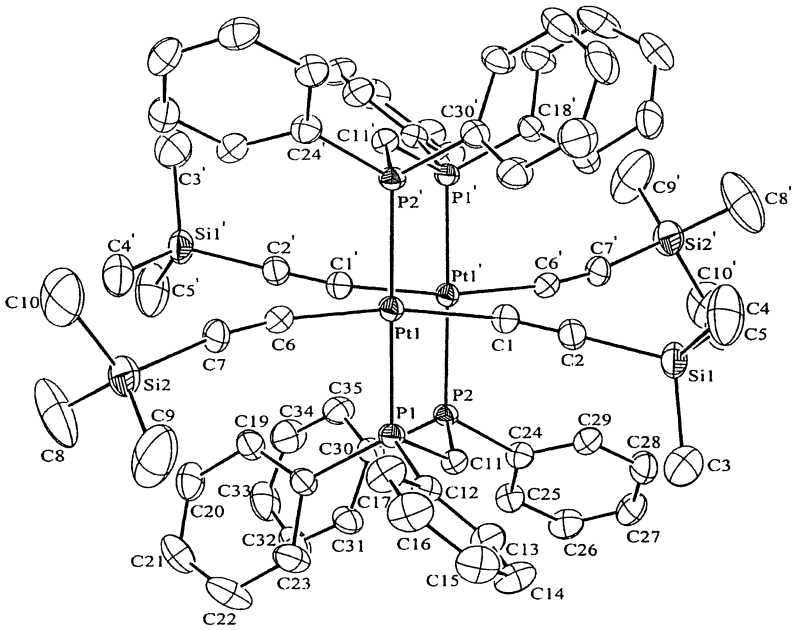

Figure 3. Perspective drawing of **3** with atomic numbering scheme. The H atoms have been omitted for clarity. Thermal ellipsoids are shown at the 30% probability level.

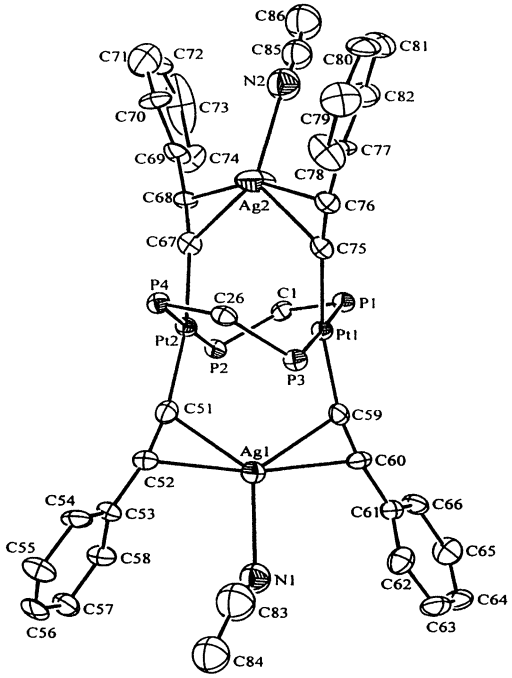

Figure 4. Perspective drawing of the complex cation of **4** with atomic numbering scheme. The H atoms and phenyl rings of dppm have been omitted for clarity. Thermal ellipsoids are shown at the 30% probability level.

ity of Ag^{I} than Cu^{I} may account for the slightly longer Pt···Pt distance in **4** than that in its copper analogue, $[Pt_2(dppm)_2(C{\equiv}CPh)_4{\cdot}\{Cu(MeCN)\}_2](PF_6)_2$.

The electronic absorption spectra of **1**−**4** show two low-energy absorption bands at ca. 318−386 and 372−415 nm, respectively, in dichloromethane solution, and their electronic absorption data are summarized in Table 4. Figure 5 depicts the electronic absorption spectra of **1**, **2**, and $[Pt_2(dppm)_2(C{\equiv}CPh)_4]$ in dichloromethane at room temperature. It is interesting to note that the nature of the alkynyl ligands, the Pt···Pt separation, and the coordination of d^{10} metal centers have an influence on the position of the low-energy absorption bands. In general, the better the π-accepting ability of the alkynyl group, the lower the energy of the low-energy absorption band. In addition, the mixed-metal complexes always show a lower energy absorption band than the dinuclear platinum(II) face-to-face precursor. With reference to the spectroscopic studies on $[Pt_2(\mu\text{-dppm})_2(CN)_4]$[1d] as well as our previous report on $[Pt_2(\mu\text{-dppm})_2(C{\equiv}CPh)_4]$,[5] in which the lowest energy absorption bands are red-shifted with respect to the respective $[d(Pt) \rightarrow \pi^*(C{\equiv}N)]$ and $[d(Pt) \rightarrow \pi^*(C{\equiv}CPh)]$ metal-to-ligand charge transfer (MLCT) transitions of their mononuclear analogues, *trans*-$[Pt(dppm)_2(CN)_2]$[9] and *trans*-$[Pt(dppm)_2(C{\equiv}CPh)_2]$,[3e,9] the low-energy absorptions in **1**−**4** are suggested to involve a transition of $[d_\sigma^*(Pt_2) \rightarrow p_\sigma(Pt_2)/\pi^*(C{\equiv}CR)]$ metal−metal-to-ligand charge transfer (MMLCT) character. The LUMO was believed to have substantial mixing of the π^* of the alkynyl group with the $p_\sigma(Pt_2)$ orbital of the Pt−Pt bonding interaction, where d_σ^* and p_σ denote the antibonding combination of the $d_{z^2}(Pt)-d_{z^2}(Pt)$ interaction and bonding combination of the $p_z(Pt)-p_z(Pt)$ interaction, respectively, taking the Pt···Pt direction as the *z*-axis. Thus, the absorption energy in the order $[Pt_2(\mu\text{-dppm})_2(C{\equiv}CPh)_4] > [Pt_2(\mu\text{-dppm})_2(C{\equiv}CC_6H_4Cl\text{-}p)_4] > [Pt_2(\mu\text{-dppm})_2(C{\equiv}CC_6H_4NO_2\text{-}p)_4]$, is in line with the π-accepting ability of RC≡C, in which R = Ph < C_6H_4-Cl-*p* < $C_6H_4NO_2$-*p*. On the other hand, the d_σ^* orbital would also be higher-lying in energy when the complex showed a stronger Pt···Pt interaction, as reflected by the shorter Pt···Pt distance observed in the X-ray crystal structure. Both effects would cause a narrowing of the HOMO−LUMO energy gap. Such a red-shift of the absorption band is in accord with the assignment of an MMLCT transition. The exceptionally large extinction coefficients observed in **2**, which are almost 5 times that of the free ligand, nitrophenyl acetylene, are suggestive

(9) (a) Yip, H. K.; Lin, H. M.; Wang, Y.; Che, C. M. *J. Chem. Soc., Dalton Trans.* **1993**, 2939. (b) Yip, H. K.; Lin, H. M.; Cheung, K. K.; Che, C. M.; Wang, Y. *Inorg. Chem.* **1994**, *33*, 1644.

Table 2. Selected Bond Distances (Å) and Angles (deg) with Estimated Standard Deviations in Parentheses

$[Pt_2(\mu\text{-dppm})_2(C{\equiv}CC_6H_4Cl\text{-}p)_4]$ (**1**)

Bond Distances (Å)

Pt(1)−P(1)	2.304(1)	C(9)−C(10)	1.194(6)
Pt(1)−P(2)	2.296(1)	P(1)−C(29)	1.837(5)
Pt(1)−C(1)	2.004(5)	P(2)−C(29)	1.829(5)
Pt(1)−C(9)	2.004(5)		
C(1)−C(2)	1.198(6)		

Bond Angles (deg)

P(1)−Pt(1)−P(2)	174.9(4)	Pt(1)−C(1)−C(2)	170.1(4)
P(1)−Pt(1)−C(1)	96.0(1)	Pt(1)−C(9)−C(10)	171.9(4)
P(1)−Pt(1)−C(9)	88.5(1)	C(1)−C(2)−C(3)	175.5(5)
P(2)−Pt(1)−C(1)	84.5(1)	C(9)−C(10)−C(11)	177.8(5)
P(2)−Pt(1)−C(9)	92.0(1)	P(1)−C(29)−P(2)	118.4(3)
C(1)−Pt(1)−C(9)	168.5(2)		

$[Pt_2(\mu\text{-dppm})_2(C{\equiv}CC_6H_4NO_2\text{-}p)_4]$ (**2**)

Bond Distances (Å)

Pt(1)−P(1)	2.306(11)	C(9)−C(10)	1.204(6)
Pt(1)−P(2)	2.312(10)	P(1)−C(24)	1.818(4)
Pt(1)−C(1)	1.992(5)	P(2)−C(36)	1.812(5)
Pt(1)−C(9)	2.018(5)		
C(1)−C(2)	1.197(6)		

Bond Angles (deg)

P(1)−Pt(1)−P(2)	176.2(1)	Pt(1)−C(1)−C(2)	176.3(4)
P(1)−Pt(1)−C(1)	91.2(1)	Pt(1)−C(9)−C(10)	172.3(4)
P(1)−Pt(1)−C(9)	85.1(1)	C(1)−C(2)−C(3)	178.2(5)
P(2)−Pt(1)−C(1)	87.4(1)	C(9)−C(10)−C(11)	174.7(5)
P(2)−Pt(1)−C(9)	96.6(1)	P(1)−C(17)−P(2)	118.1(3)
C(1)−Pt(1)−C(9)	172.1(2)		

$[Pt_2(\mu\text{-dppm})_2(C{\equiv}CSiMe_3)_4]$ (**3**)

Bond Distances (Å)

Pt(1)−P(1)	2.294(16)	C(6)−C(7)	1.188(10)
Pt(1)−P(2)	2.307(16)	P(1)−C(11)	1.840(7)
Pt(1)−C(1)	2.024(7)	P(2)−C(11)	1.838(7)
Pt(1)−C(6)	2.017(7)		
C(1)−C(2)	1.193(10)		

Bond Angles (deg)

P(1)−Pt(1)−P(2)	175.7(1)	Pt(1)−C(1)−C(2)	168.1(6)
P(1)−Pt(1)−C(1)	84.7(2)	Pt(1)−C(6)−C(7)	167.9(7)
P(1)−Pt(1)−C(6)	86.7(2)	C(1)−C(2)−Si(1)	176.3(7)
P(2)−Pt(1)−C(1)	94.2(2)	C(6)−C(7)−Si(2)	171.4(7)
P(2)−Pt(1)−C(6)	95.3(2)	P(1)−C(11)−P(2)	119.5(3)
C(1)−Pt(1)−C(6)	163.2(3)		

$[Pt_2(\mu\text{-dppm})_2(C{\equiv}CPh)_4{\cdot}\{Ag(MeCN)\}_2](BF_4)_2$ (**4**)

Bond Distances (Å)

Pt(1)−P(1)	2.336(3)	Ag(1)−C(51)	2.353(10)
Pt(1)−P(3)	2.322(3)	Ag(1)−C(52)	2.412(11)
Pt(1)−C(75)	2.006(12)	Ag(1)−C(59)	2.354(12)
Pt(1)−C(59)	2.047(12)	Ag(1)−C(60)	2.433(12)
C(59)−C(60)	1.186(15)	Ag(1)−N(1)	2.390(4)
C(51)−C(52)	1.204(19)	Ag(2)−N(2)	2.420(4)
P(1)−C(1)	1.816(1)	N(1)−C(83)	1.13(6)
P(2)−C(1)	1.827(1)	N(2)−C(85)	1.22(6)

Bond Angles (deg)

P(1)−Pt(1)−P(3)	177.9(1)	Pt(1)−C(75)−C(76)	168.0(9)
P(1)−Pt(1)−C(75)	96.9(4)	Pt(2)−C(51)−C(52)	169.6(9)
P(1)−Pt(1)−C(59)	86.5(4)	C(59)−C(60)−C(61)	169.9(12)
P(3)−Pt(1)−C(75)	83.3(4)	C(75)−C(76)−C(77)	172.3(12)
P(3)−Pt(1)−C(59)	93.7(4)	N(1)−Ag(1)−C(51)	125.2(8)
C(59)−Pt(1)−C(75)	168.0(4)	N(2)−Ag(2)−C(67)	126.3(8)

of the addition effect of the extinction coefficients of the four $C{\equiv}CC_6H_4NO_2\text{-}p$ units and the mixing of the intraligand (IL) $\pi \rightarrow \pi^*(C{\equiv}CC_6H_4NO_2\text{-}p)$ transition into the MMLCT transition. Figure 6 shows the electronic

Table 3. Pt···Pt Distances of Dinuclear Pt(II) Alkynyl Complexes

complex	d(Pt···Pt), Å
$[Pt_2(\mu\text{-dppm})_2(C{\equiv}CC_6H_4Cl\text{-}p)_4]$ (**1**)	3.340
$[Pt_2(\mu\text{-dppm})_2(C{\equiv}CC_6H_4NO_2\text{-}p)_4]$ (**2**)	3.250
$[Pt_2(\mu\text{-dppm})_2(C{\equiv}CSiMe_3)_4]$ (**3**)	3.349
$[Pt_2(dppm)_2(C{\equiv}CPh)_4{\cdot}\{Ag(MeCN)\}_2](BF_4)_2$ (**4**)	3.064
$[Pt_2(dppm)_2(C{\equiv}CPh)_4]$[a]	3.437
$[Pt_2(dppm)_2(C{\equiv}CPh)_4{\cdot}\{Cu(MeCN)\}_2](PF_6)_2$[a]	3.012

[a] From ref 5.

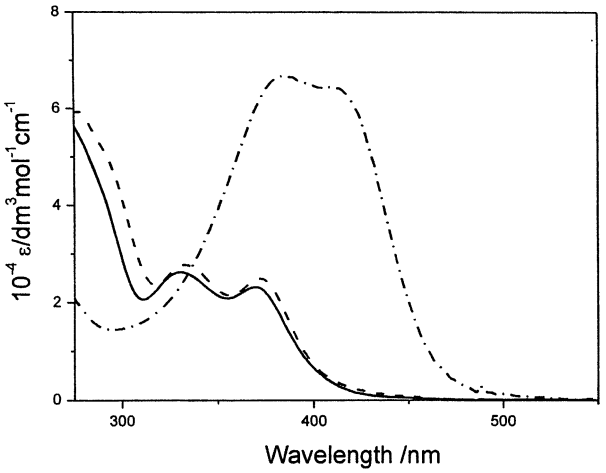

Figure 5. Electronic absorption spectra of $[Pt_2(\mu\text{-dppm})_2(C{\equiv}CPh)_4]$ (—), **1** (- − -), and **2** (- · - · -) in dichloromethane solution at 298 K.

absorption spectra of **4**, $[Pt_2(\mu\text{-dppm})_2(C{\equiv}CPh)_4{\cdot}\{Cu(MeCN)\}_2](PF_6)_2$, and $[Pt_2(dppm)_2(C{\equiv}CPh)_4]$ in dichloromethane at room temperature. Similarly, the red-shift of the absorption band upon encapsulation of silver(I) ions in **4** (354 and 400 nm) and $[Pt_2(dppm)_2(C{\equiv}CPh)_4{\cdot}\{Cu(MeCN)\}_2](PF_6)_2$ (372 and 419 nm) compared to its precursor complex, $[Pt_2(dppm)_2(C{\equiv}CPh)_4]$ (330 and 370 nm), can be ascribed to the narrower HOMO−LUMO energy gap as a consequence of an increase in the alkynyl π-acceptor ability as well as the stronger Pt···Pt interaction. The higher absorption energy of the bands observed in **4** relative to its copper(I) analogue, $[Pt_2(dppm)_2(C{\equiv}CPh)_4{\cdot}\{Cu(MeCN)\}_2](PF_6)_2$, is ascribed to the weaker acidity of Ag^I than Cu^I. The stronger Lewis acidity of Cu^I and the shorter Pt···Pt distance in $[Pt_2(dppm)_2(C{\equiv}CPh)_4{\cdot}\{Cu(MeCN)\}_2](PF_6)_2$ would lower the $\pi^*(C{\equiv}CPh)$ orbital energy as well as raise the d_σ^* orbital energy, leading to a lowering of its MMLCT transition energy.

Upon excitation at $\lambda > 350$ nm, **1**−**4** exhibit strong luminescence in the solid state both at room temperature and at 77 K and in room-temperature fluid solution. The photophysical data of **1**−**4** together with their related complexes are shown in Table 4. Room-temperature emission spectra in dichloromethane show an emission band at ca. 620−664 nm. Figure 7 shows the emission spectra of **1** and **2** in room-temperature dichloromethane solution. Similar to the electronic absorption spectra, the energy dependence of the emission band on the nature of the alkynyl group, together with the previous spectroscopic works on related d^8−d^8 dinuclear systems[5,9] and the close resemblance of the excitation maxima to the low-energy absorption bands, are suggestive of an emission of ^{3}MMLCT origin. The observation of a lower emission energy in **1** (628 nm) and **2** (664

Table 4. Electronic Absorption and Emission Data

	absorption[a]	emission	
complex	λ/nm (ϵ_{max}/dm^3 mol^{-1} cm^{-1})	medium (T/K)	λ_{em}/nm (τ_o/μs)
1	276 (52,110), 334 (23,940), 374 (21,250)	CH_2Cl_2 (298)	628 (1.3 ± 0.1)
		solid (298)	575[c] (6.2 ± 0.2)
		solid (77)	575 (6.7 ± 0.3)
		glass[a] (77)	485 (3.1 ± 0.2), 566[d] (19.8 ± 0.3)
2	386 (66,980), 415 (64,040)	CH_2Cl_2 (298)	664 (1.3 ± 0.1)
		solid (298)	574[c] (<0.1)
		solid (77)	574 (6.4 ± 0.1)
		glass[a] (77)	566 (69.5 ± 0.5), 595[d] (91.6 ± 0.5)
3	274 (11,080), 318 (14,380), 372 (7470)	CH_2Cl_2 (298)	630 (<0.1)
		solid (298)	*e*
		solid (77)	595[c] (<0.1)
		glass[a] (77)	477 (<0.1), 594[d] (<0.1)
4	354 (32,040), 400 sh (10,780)	CH_2Cl_2 (298)	622 (<0.1)
		solid (298)	470 (<0.1), 615 (1.9 ± 0.2)
		solid (77)	465 (1.5 ± 0.1), 620 (4.3 ± 0.4)
		glass[b] (77)	460 (2.9 ± 0.3), 600[d] (7.7 ± 0.8)
$[Pt_2(\mu\text{-dppm})_2(C{\equiv}CC_6H_5)_4]$[f]	270 (56,810), 330 (28,890), 370 (25,540)	CH_2Cl_2 (298)	620 (<0.1)
		solid (298)	580 {615}[c] (<0.1)
		solid (77)	607 (6.0 ± 0.6)
		glass[a] (77)	460 (3.4 ± 0.3), 545[d] (8.2 ± 0.8)
$[Pt_2(dppm)_2(C{\equiv}CPh)_4{\cdot}\{Cu(MeCN)\}_2](PF_6)_2$[f]	372 (33,160), 418 (18,350)	CH_2Cl_2 (298)	625 (0.22 ± 0.02)
		solid (298)	495 (<0.1), 610 (2.2 ± 0.2)
		solid (77)	490 (4.1 ± 0.4), 634 (6.1 ± 0.6)
		glass[b] (77)	476 (2.0 ± 0.2), 590[d] (8.9 ± 0.9)

[a] In CH_2Cl_2. [b] In EtOH−MeOH (4:1 v/v), emission maxima are recorded by time-resolved emission measurement. [c] In crystal form before rigorous drying. [d] Vibronic-structured with vibrational progressional spacings of 2190−2220 cm^{-1}. [e] Not emissive. [f] From ref 5.

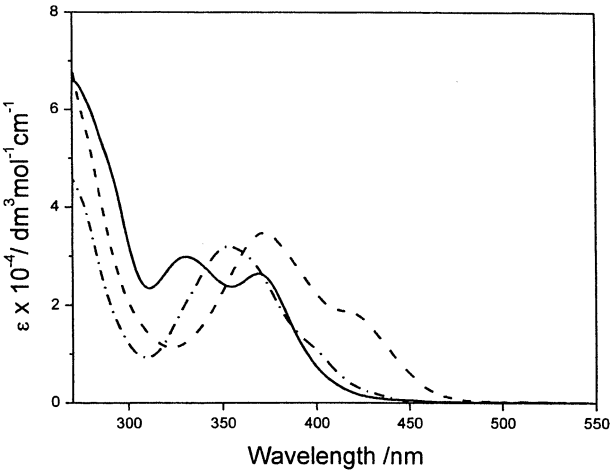

Figure 6. Electronic absorption spectra of $[Pt_2(\mu\text{-dppm})_2(C{\equiv}CPh)_4]$ (—), $[Pt_2(\mu\text{-dppm})_2(C{\equiv}CPh)_4\{Cu(MeCN)\}_2]^{2+}$ (- − -), and **4** (- · - · -) in dichloromethane at 298 K.

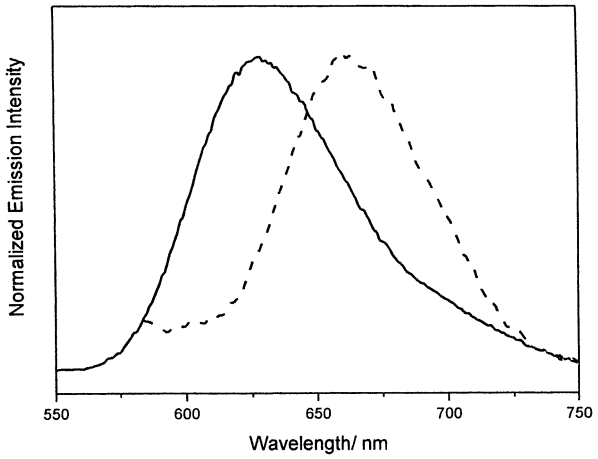

Figure 7. Emission spectra of **1** (—) and **2** (- − -) in degassed dichloromethane at 298 K.

nm) compared to that in $[Pt_2(\mu\text{-dppm})_2(C{\equiv}CPh)_4]$ (620 nm) is attributed to the lower $\pi^*(C{\equiv}CR)$ orbital energy due to the presence of the electron-withdrawing chloro and nitro substituent. Mixing of an intraligand (IL) character into the ^{3}MMLCT state cannot be completely ruled out for **2** in the presence of the highly electron-deficient nitrophenyl-substituted alkynyl ligand. In the solid state and glass state at 77 K, two emission bands were found at ca. 460−500 and 545−634 nm, and these emission bands are believed to be of different origins on the basis of their large energy separation and difference in excited-state lifetimes. The higher energy emission was tentatively assigned as intraligand phosphorescence. In view of the vibrational progressional spacings of ca. 2000−2200 cm^{-1}, which is typical of the $\nu(C{\equiv}C)$ stretch in the ground state, the lower energy vibronic-structured emission band is assigned as originated from the ^{3}MMLCT state. The 77 K emission spectrum of **1** is shown in Figure 8. The lower emission energy of **4** than the precursor complex in 77 K glass is consistent with this ^{3}MMLCT assignment. The coordination of the Ag^I ion will shorten the Pt···Pt distance since the bending of the C−Pt−C bond will force the two Pt centers into closer proximity. This, together with the reduction of electron density at the Pt center as a result of an increase in π-accepting ability of the PhC≡C groups upon π-donation to Ag^I, would bring the two Pt centers into close proximity. Both the contraction of the Pt···Pt distance and the increase in π-accepting ability of the alkynyl group would result in a narrowing of the HOMO−LUMO energy gap, and hence a lower emission energy of **4** was observed, again consistent with the findings in the electronic absorption studies. The slightly higher emission energy of the

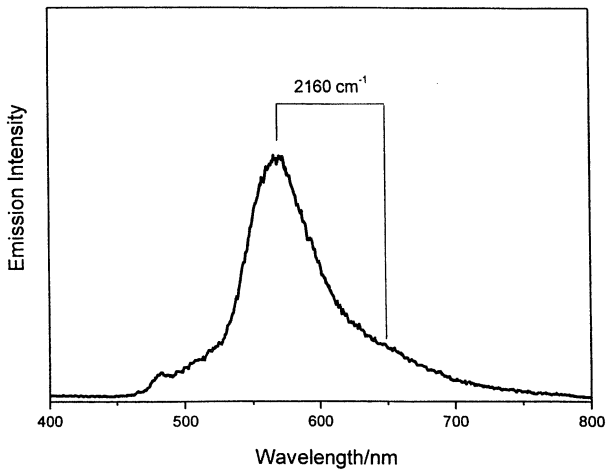

Figure 8. Time-resolved emission spectrum of **1** in dichloromethane at 77 K recorded 29 μs after the laser flash excitation.

mixed-metal complex, **4**, than its copper analogue has been ascribed to the weaker Lewis acidity of Ag^I as well as the larger ionic radius of Ag^I than Cu^I, which raises the π^*(C≡CPh) orbital energy and lowers the d_σ^* orbital energy, leading to higher MMLCT transition energy in **4**.

Acknowledgment. V.W.-W.Y. acknowledges support from The University of Hong Kong Foundation for Educational Development and Research Limited and the receipt of a Croucher Senior Research Fellowship from the Croucher Foundation. The work described in this paper has fully been supported by a CERG grant from the Research Grant Council of the Hong Kong Special Administrative Region, People's Republic of China (Project No. HKU7123/00P). C.-K.H. acknowledges the receipt of a postgraduate studentship, and K.M.-C.W. and N.Z. acknowledge the receipt of University Postdoctoral Fellowships, both administered by The University of Hong Kong.

Supporting Information Available: Tables of atomic coordinates, thermal parameters, and a full list of bond distances and angles for **1**, **2**, **3**, and **4** are deposited as Supporting Information. This material is available free of charge via the Internet at http://pubs.acs.org.

OM020093O